Band offsets of a ruthenium gate on ultrathin high-κ oxide films on silicon

Sylvie Rangan, Eric Bersch, and Robert Allen Bartynski
Department of Physics and Astronomy and Laboratory for Surface Modification, Rutgers University, 136 Frelinghuysen Road, Piscataway, New Jersey 08854, USA

Eric Garfunkel
Department of Chemistry and Chemical Biology and Laboratory for Surface Modification, Rutgers University, 610 Taylor Road, Piscataway, New Jersey 08854, USA

Elio Vescovo
National Synchrotron Light Source, Brookhaven National Laboratory, Upton, New York 11973, USA
(Received 29 August 2008; revised manuscript received 2 December 2008; published 9 February 2009)

Valence-band and conduction-band edges of ultrathin oxides (SiO_2, HfO_2, $Hf_{0.7}Si_{0.3}O_2$, and Al_2O_3 grown on silicon) and their shifts upon sequential metallization with ruthenium have been measured using synchrotron-radiation-excited x-ray, ultraviolet, and inverse photoemissions. From these techniques, the offsets between the valence-band and conduction-band edges of the oxides, and the ruthenium metal gate Fermi edge have been directly measured. In addition the core levels of the oxides and the ruthenium have been characterized. Upon deposition, Ru remains metallic and no chemical alteration of the underlying oxide gates, or interfacial SiO_2 in the case of the high-κ thin films, can be detected. However a clear shift of the band edges is measured for all samples due to the creation of an interface dipole at the ruthenium-oxide interface. Using the energy gap, the electron affinity of the oxides, and the ruthenium work function that have been directly measured on these samples, the experimental band offsets are compared to those predicted by the induced gap states model.

DOI: 10.1103/PhysRevB.79.075106 PACS number(s): 77.55.+f, 73.40.Qv, 82.80.Pv

I. INTRODUCTION

Scaling of metal-oxide-semiconductor (MOS) structures has reached the point where replacement of the traditional SiO_2 gate oxide and the polysilicon gate electrode by alternative materials is needed to maintain device performance.[1,2] SiO_2 has a physical limitation of ~1 nm because the large leakage current through the oxide results in an unacceptably high power consumption and poor control of the channel. Addressing this problem by replacing SiO_2 with a physically thicker alternative dielectric that has a higher dielectric constant (high κ) had met with some success. Such a structure maintains a high capacitance while lowering the leakage current. Most high-κ dielectrics (such as those explored in this work) however have band gaps that are smaller than the SiO_2 band gap. This property makes the alignment of the valence-band (VB) and conduction-band (CB) edges of the dielectric with those of the semiconductor substrate, as well as with the Fermi level (E_F) of the metal gate, a critical issue. To maintain a low leakage current, band offsets of at least 1 eV are required.[1,3] The choice of the dielectric is also limited by important factors such as the quality of the interface between the gate oxide and the semiconducting channel, the chemical stability of the system upon the high-temperature anneal necessary for dopant activation, and the presence of intrinsic defects in the gate oxide films. Among the leading candidates to replace SiO_2 are HfO_2, $Hf_xSi_{1-x}O_2$, and their nitrided analogs. While some of these materials have already been incorporated in commercially produced devices, many fundamental questions remain as to what determines band alignment in these systems, and what are the limitations of models currently used to predict band alignment.

Replacing SiO_2 with high-κ dielectrics without also replacing the Si-based gates (highly doped polysilicon) used as electrode materials may not be sufficient for device scaling. PolySi gates exhibit the depletion of carriers near gate-oxide interface, causing an increase in capacitance that is equivalent to a ~0.3 nm increase in SiO_2 dielectric thickness. When compared to the typical 1.2 nm thickness of the oxide gate needed for advanced complementary MOS (CMOS) applications, this effect is considerable. Although different semiconductor manufacturers have different approaches and solutions to the critical technological problem, metal gates are being investigated to replace polySi gates and, like high-κ dielectrics, have recently entered commercial applications. The development of dual work function metal gate [i.e., a low work function metal (~4.1 eV) for *n*-MOS and a high work function metal (~5.2 eV) for *p*-MOS] is the preferred solution to keeping a small threshold voltage; thus the Fermi level of the two metal should match the silicon band edges.[4] Aside from work function compatibility, chemical stability of metal-dielectric system, especially upon annealing, raises other issues such as metal oxidation and defect creation in the dielectric layer. Owing to its high work function, Ru is an interesting candidate metal for *p*-MOS applications. Although other metals (compounds) will likely see more extensive use in commercial applications,[5] Ru is a good choice for model studies of band alignment because of its relatively low oxygen affinity, which will maintain the stack integrity upon Ru metallization.

To address the question of band alignment between a Ru gate and the oxide substrate, it is necessary to define several parameters. Figure 1 shows a generic energy-band diagram of a metal-oxide-semiconductor stack, where the gate metal (Ru here) is the outer layer. In this diagram, the vacuum level is in principle meaningful only for the outer Ru layer as the substrate and the oxide are buried. Nevertheless, representing

 ©2009 The American Physical Society

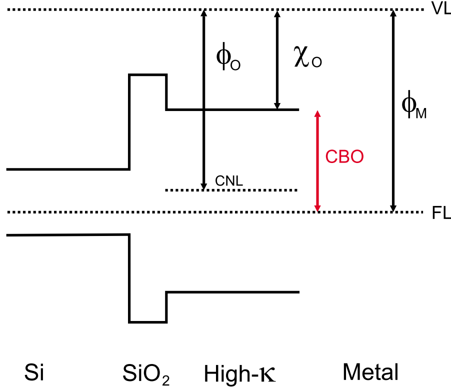

FIG. 1. (Color online) Schematic representation of band alignment across a metal/high-κ/SiO_2/Si structure.

the vacuum level for the oxide is useful in defining several oxide parameters: the electron affinity, χ_O, is defined as the difference between the conduction-band minimum and the vacuum level, and the oxide effective work function, ϕ_O, is defined as the difference between the vacuum level and the charge neutrality level (CNL) of the oxide.[3,6] The CNL of an oxide is defined as the energy in the band gap where evanescent states have an equal weight of the valence-band and conduction-band characters.[7,8] The metal work function ϕ_M is defined as the difference between the vacuum level and the Fermi level of the metal.

To predict the band alignment at a metal-oxide interface, two models that represent two extremes of interaction can be considered. In the Schottky-Mott model, where it is assumed that there is no interaction or charge rearrangement at the interface between the metal and oxide, the metal-oxide junction behaves as two independent noninteracting solids. As a consequence, the energy-band alignment is given by the alignment of the common vacuum levels of the two materials.[9,10] In terms of the parameters defined above, the conduction-band offset (CBO) (as shown in Fig. 1) between the oxide conduction band and the metal Fermi level is therefore given by

$$\mathrm{CBO} = \phi_M - \chi_O. \quad (1)$$

The other extreme is the Bardeen limit where the electronic response to the perturbation created by the junction is dominant and, in the absence of an "extrinsic" pinning level, the band alignment is driven by the alignment of the metal Fermi level with the oxide CNL.[11,12] In this limit, the conduction-band offset is given by

$$\mathrm{CBO} = \phi_O - \chi_O. \quad (2)$$

The actual behavior of most metal or oxide junctions falls between these two extremes. To account for this behavior, the metal induced gap states (MIGS) model was developed.[7,8] In this model, the conduction-band offset is given by

$$\mathrm{CBO} = S(\phi_M - \phi_O) + (\phi_O - \chi_O), \quad (3)$$

where S is the so-called pinning parameter of the oxide.

The S parameter can be related to the dielectric constant of the oxide and can vary from zero to one.[13] For a number of oxides, S and the position of the CNL have been theoretically calculated.[3,6] In principle, taking these calculated parameters along with experimental measurements of ϕ_M, χ_O, and the oxide gap, the CBO between the metal Fermi level and the oxide conduction-band minimum can be predicted.

In this work, we investigate the evolution of band offsets upon sequential Ru metallization of different ultrathin oxides (SiO_2, HfO_2, $Hf_{0.7}Si_{0.3}O_2$, and Al_2O_3) grown on a silicon substrate. The measurements were performed at room temperature in UHV with the combined use of ultraviolet photoemission spectroscopy (UPS) (to probe the occupied electronic states) and inverse photoemission spectroscopy (IPS) (to probe the unoccupied electronic states). This approach allows the direct measurement of the band gap and band offsets (with respect to the substrate Si and with respect to the metal Fermi level) of these films in a single experimental chamber.[14] With these measurements we have investigated both the valence-band and conduction-band densities of states, as well as extracted the electron affinity of the oxide films and the Ru work function. In addition, we have performed synchrotron-excited soft x-ray photoemission studies of the same Ru-metallized samples in an effort to characterize the shallow core levels of these systems, and to investigate the chemical state of the oxide films and metal gate during sequential Ru deposition. For all these systems, the measured band offsets between the oxide and the Ru gate are found to be in good agreement with the MIGS model.

II. EXPERIMENTAL METHODS

A. Spectroscopic techniques

The majority of measurements presented here were obtained using a single ultrahigh vacuum experimental chamber that housed instrumentation for both UPS and IPS. The base pressure of the chamber was less than 5×10^{-10} Torr. Valence-band photoelectrons were excited using a Leybold-Heraeus helium discharge photon source (HeI: 21.2 eV and HeII: 40.8 eV), and energy analysis of the emitted electrons was performed in an angle-integrated mode using a double pass Phi 15–255G cylindrical mirror analyzer (CMA). The axes of the photon source and the CMA formed a 90° angle, and the sample normal was oriented midway between the two. By applying a −5 V bias to the sample under exposure to HeI radiation, the entire width of the photoemission spectrum was measured and the binding energy of the valence-band maximum (VBM) with respect to the vacuum level was determined. From this information, and a direct measurement of the energy gap, χ_O and ϕ_M was made.

Inverse photoemission spectra were obtained using a grating spectrometer, described in detail elsewhere,[15] which was mounted on the same experimental chamber. Briefly, a well-collimated monoenergetic electron beam (primary energy E_p=20.3 or 23.3 eV in this study) was directed toward the sample along the surface normal. The electrons couple to high-lying unoccupied states and a subset relaxes via a direct optical transition to low lying unoccupied states in the conduction band, emitting a photon in the process. The photons

were dispersed by a concave spherical diffraction grating and detected by a microchannel plate with position sensitive resistive anode encoder. With this approach, the intensity of photons as a function of photon energy reflects the density of unoccupied states in the conduction band. As our samples were amorphous, both UPS and IPS spectra were effectively angle integrated, and our measurements yield the oxide band gaps. In our photoemission and inverse photoemission spectra, the VBM and the conduction-band maximum (CBM) are both measured with respect to the Fermi level of a gold sample. The overall energy resolution for the UPS and IPS spectra is estimated to be 0.25 eV.

Soft x-ray photoemission spectroscopy (SXPS) has been performed on the U5UA beamline at the National Synchrotron Light Source[16] to study both the shallow core levels, and the valence band of metal/oxide/semiconductor stacks. Photoelectrons were collected with an Omicron 125 mm hemispherical electron energy analyzer with an angular resolution of $\pm 1°$ oriented along the sample normal. The photon beam impinged on the sample at an angle of 45°. Spectra were taken at a 150 eV photon energy with an instrumental energy resolution of 0.1 eV. The pressure in the analysis chamber was always better than 1×10^{-10} Torr.

In this work, the energy scale of all x-ray photoemission spectroscopy (XPS), UPS, and IPS spectra is referenced to the experimental silicon midgap (approximated to 0.6 eV above the experimentally measured silicon valence-band maximum). The choice of referencing the spectra to the silicon midgap prior to Ru metallization is motivated by the necessity to compare the core levels of pristine samples with different doping levels or different pinnings. Our energy reference is equivalent to referencing to the Fermi level (that we measure experimentally on a gold or silver foil in contact with the sample) but adding a different offset for each sample to account for the (different) initial Fermi-level pinning. After Ru deposition, band bending in the silicon substrate can occur. We do not readjust the energy scale to the silicon midgap after each Ru deposition. Energy shifts that bring the VBM closer to E_F and move the CBM farther above E_F are defined as positive-energy shifts.

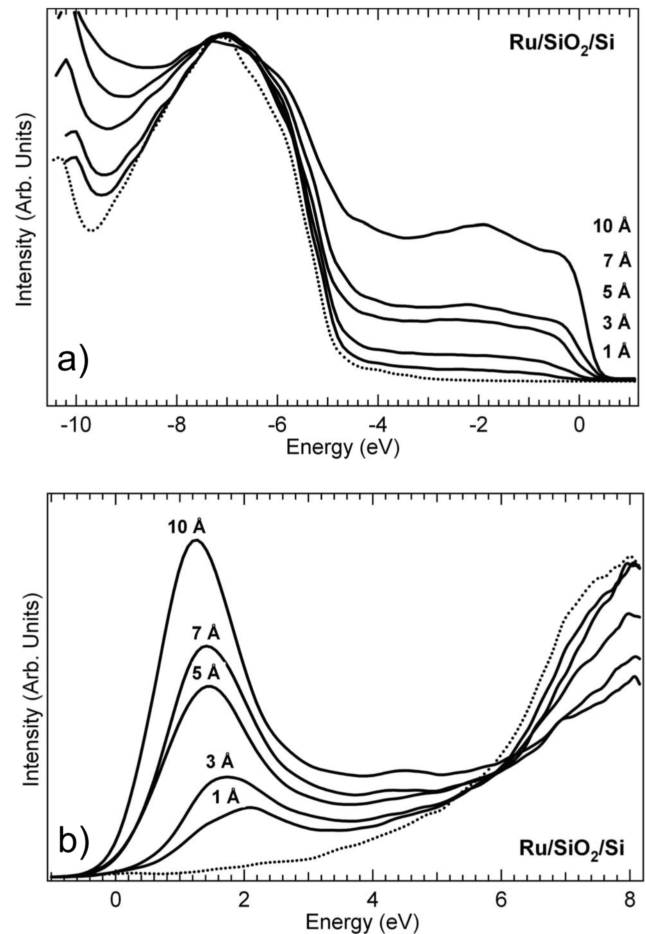

FIG. 2. (a) UPS ($h\nu$=40.8 eV) and (b) IPS (E_p=23.3 eV) spectra of the VB and CB band edges, respectively, during sequential metallization of a 20 Å SiO_2/Si with Ru. The spectra are referenced with respect to the silicon midgap position of the pristine sample.

B. Sample treatment and metallization

All of the dielectric films measured in this study were grown on single-crystal Si(100) surfaces and transported in air to our spectroscopic chambers. Thin films in the thickness range of 15–30 Å of HfO_2, $Hf_{0.7}Si_{0.3}O_2$, SiO_2, and Al_2O_3 were examined. Details regarding film preparation are outlined in an earlier work.[14] Upon insertion into the experimental chamber, the samples were cleaned by resistive heating to about 500 °C for several minutes. This treatment has proven to be critical in order to avoid the growth of spectral features within the band gap of the dielectric during measurements, most likely owing to reaction between adsorbed species and the dielectric film that were induced by the IPS electron beam.[14]

Ru (99.9% purity) was deposited *in situ* using a well-outgassed electron-beam evaporation source, with a pressure lower than 5×10^{-9} Torr. The thickness of deposited Ru was monitored by a quartz-crystal monitor (QCM) positioned just below the sample. The QCM was calibrated using Rutherford backscattering spectrometry. The cleanliness of the starting surface and the deposited metal was determined by Auger-electron spectroscopy (AES) or XPS, and indicates no contaminations or oxidation above the detection limit of a maximum of 5% of the techniques.

C. Band edge determination

In our XPS, UPS, and IPS spectra, the use of thin dielectric films results in contributions from both the valence and conduction bands of the substrate Si. To determine the band edge of the dielectric, we account for this extra emission by assuming a linear contribution from the silicon substrate. While in principle it might be preferable to subtract the appropriately scaled line shape of the elemental Si valence band, typically the substrate contribution is so small that a linear assumption does not introduce a significant error.[14] The error for the energy determination of the band edges is estimated to 0.1 eV.

The values of χ_O for the clean oxides and ϕ_M for the Ru films were determined from HeI excited UPS spectra ob-

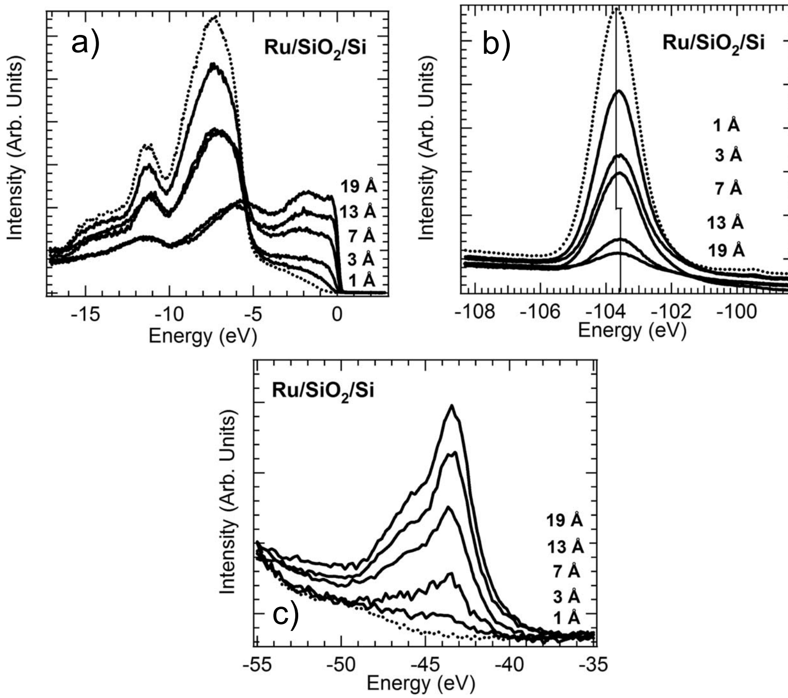

FIG. 3. (a) Valence-band, and (b) Si $2p$ and (c) Ru $4p$ core levels spectra measured at a photon energy $h\nu$=150 eV of a 20 Å SiO_2/Si sample before and during sequential metallization with Ru. The spectra are referenced with respect to the silicon midgap position of the pristine sample.

tained with a −5 V bias on the sample. The total width of the spectrum, W, was extracted using a linear extrapolation of the data to the background intensity level at both the high-kinetic-energy and low-kinetic-energy ends of the spectrum. These parameters χ_O and ϕ_M were then obtained as

$$\chi_O = h\nu - W - E_{gap}, \quad (4)$$

$$\phi_M = h\nu - W, \quad (5)$$

where $h\nu$ is the photon source energy, and E_{gap} is the gap of the high-κ dielectric film as determined from combined UPS and IPS measurements.

III. RESULTS

A. Ru/20 Å SiO_2/Si

The SiO_2 sample used in this study was a 20 Å thermal oxide grown on a n-doped Si with a resistivity of 70 Ω cm^{-1}.

Figures 2(a) and 2(b) present UPS and IPS spectra of the valence (measured at a photon energy $h\nu$=40.8 eV) and conduction bands (measured at an electron energy E_p =23.3 eV), respectively, upon sequential Ru metallization of the 20 Å SiO_2/Si film. The energy scales of the figures are referenced to the silicon midgap of the pristine sample. In the figures, the Ru thickness is indicated for the spectra obtained at each metallization cycle. For the clean oxide surface (dotted lines), the valence-band (mostly of O $2p$ character) and conduction-band (a mixture of Si $4s$ and Si $3p$ characters) edges are −5.1 and +3.8 eV with respect to the silicon midgap position, respectively, as we determined in a previous study.[14] Due to the strong cross section of the Ru $4d$ states, even for small Ru coverage, significant emission appears both above and below the Fermi level, and a strong and characteristic metallic Fermi edge develops. (Note that as the zero energy is chosen at the silicon midgap position of the pristine sample, the inflection point of the metallic Fermi edge does not necessary coincide with the zero of energy.) An important point of this series of metallization spectra is that a small shift toward the positive energies can be observed between the band edges of the clean oxide spectrum and those of the spectrum from the smallest Ru coverage. This shift is approximately 0.2 eV at both edges. However, as Ru states are adding spectral weight near the band edges of the oxide, a more precise way to make a quantitative determination of the band shift is to monitor changes in the SXPS spectra of the oxide core levels.

SXPS spectra of the valence band, and the Si $2p$ and the Ru $4p$ core levels of the Ru/SiO_2/Si system measured at a photon energy of $h\nu$=150 eV, are presented in Figs. 3(a)–3(c), respectively. Spectra from both the clean oxide (dotted line) and the oxide after sequential metallizations with Ru (continuous lines) are shown. The shape of the valence band shown in Fig. 3(a), characterized by greater intensity near the Fermi edge with increasing Ru coverage and a small shift of the valence band to higher energy, is similar to the spectra of Fig. 2(a). However, the magnitude of this band shift can be better estimated from the Si $2p$ core levels shown in Fig. 3(b). The clean SiO_2 Si $2p$ core level is characteristic of a Si^{4+} oxidation state, where the Si $2p_{3/2}$ peak (obtained after deconvolution, assuming a Si $2p_{1/2}$:Si $2p_{3/2}$ ratio of 0.5 and 0.6 eV spin-orbit splittings) is found at an energy of 103.7 eV with respect to the silicon midgap of the pristine sample. After the first Ru deposition, the Si $2p$ peak appears to be rigidly shifted by 0.2 eV toward higher energy. For higher Ru coverages, the Si $2p$ peak position is fixed at this new value and the line shape is unaffected by the Ru deposition. This latter observation indicates that no strong chemical interaction occurs between the Ru with the SiO_2 substrate. Furthermore, the Ru $4p$ core levels shown in Fig.

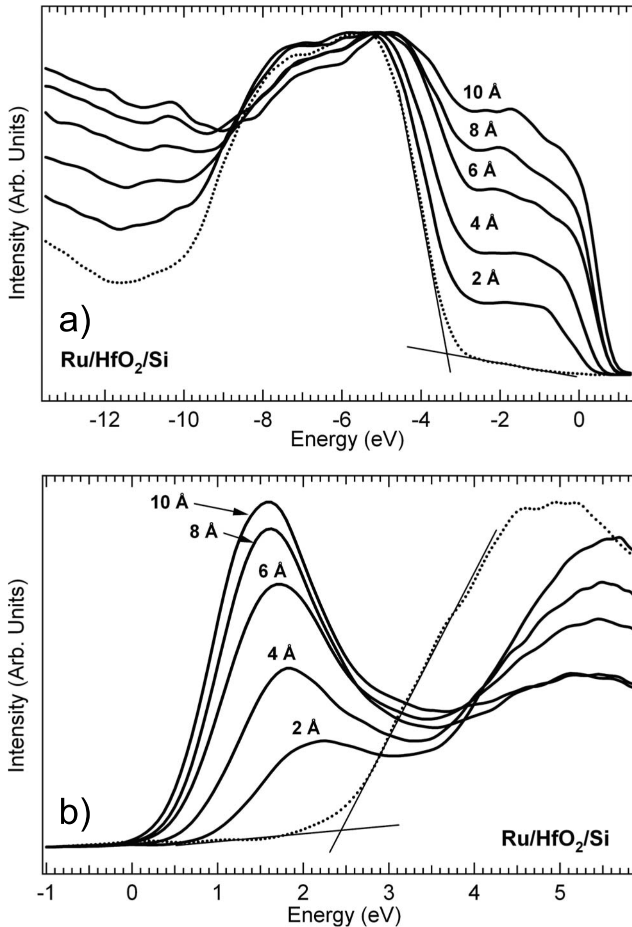

FIG. 4. (a) UPS ($h\nu$=40.8 eV) and (b) IPS (E_p=20.3 eV) spectra of the VB and CB band edges, respectively, during sequential metallization of a 15 Å HfO_2/Si with Ru. The spectra are referenced with respect to the silicon midgap position of the pristine sample.

3(c) are characteristic of metallic Ru. The core levels can be decomposed into two Ru $4p_{1/2}$ and Ru $4p_{3/2}$ Voight components of 3.5 and 2.7 eV full width at half maximum (FWHM), centered at −46.4 and −43.5 eV (0.8 eV Gaussian, and 3.3 and 2.5 eV Lorentzian), respectively. The area ratio Ru $4p_{1/2}$:Ru $4p_{3/2}$ is close to 0.4, consistent with studies in the literature.[17] These properties confirm that during sequential Ru deposition onto SiO_2 at room temperature, Ru is not oxidized.

To summarize these results, upon metallic Ru deposition, a rigid shift of +0.2 eV can be observed for all the SiO_2 related features, and is not related to any chemical alteration of the SiO_2.

B. Ru/15 Å HfO_2/Si

The HfO_2 sample studied here was 15 Å thick and was grown by the IBM company by atomic layer deposition (ALD) on a p-doped Si with a resistivity of 1–2 Ω cm^{-1}.

Valence-band photoemission spectra and IPS spectra of the conduction band of the HfO_2/Si system upon increasing metallization with Ru are shown in Figs. 4(a) and 4(b), respectively. The UPS spectrum was obtained with 40.8 eV photons and IPS spectra were obtained with an electron energy of E_p=20.3 eV. Spectra from the clean oxide surface are shown as the dotted lines in each figure. The HfO_2 electronic structure is characteristic of a transition-metal oxide. For the clean oxide surface, the valence band is mostly of O 2p character and exhibits a strong edge that when fit with a linear function projects to a VBM of 3.3 eV below the silicon midgap position.[14] The conduction band is dominated by Hf 5d states, resulting in a strong contribution in IPS. A linear fit to the low energy edge gives a CBM of 2.4 eV above the silicon midgap position.[14] With these values, the oxide band gap is measured to be 5.7 eV. After the first Ru deposition (estimated to be the equivalent of 2 Å), intensity from both the occupied and unoccupied Ru 5d states develop near the Fermi level and a strong positive-energy shift of the bands is observed. By estimating the change in the VB and CB edges, a shift between 0.4 eV and 0.5 eV is estimated. Similar to the procedure used above to determine energy shifts upon Ru metallization of SiO_2, examination of the Hf 4f oxide core levels can give the most reliable estimate of the band shift.

Soft x-ray valence-band spectra, and Hf 4f, Ru 4p, and Si 2p core-level spectra, measured at a photon energy of $h\nu$=150 eV, are reported in Figs. 5(a)–5(c), respectively. Spectra from both the clean (dotted curves) and Ru-metallized (solid curves) oxide surfaces are shown. The line shape of the VB measured at $h\nu$=150 eV is comparable to what was obtained at $h\nu$=40.8 eV. A positive shift of the VB is clearly visible and the Ru-induced intensity develops a strong Fermi edge. The line shapes of the Hf $4f_{5/2}$ and Hf $4f_{7/2}$ core-level spectra of Fig. 5(b) can be fit with two Voight line shapes at 19.2 and 17.5 eV, respectively, both with an energy width of 1.0 eV (1.0 eV Gaussian and 0.2 eV Lorentzian). These values are comparable to those previously reported in the literature.[18] Once again, the general shape of this core level appears unchanged upon Ru deposition but the lines exhibit a rigid shift of +0.5 eV after the first Ru deposition. As the Ru 4p core levels of Fig. 5(c) can be decomposed into two Ru $4p_{1/2}$ and Ru $4p_{3/2}$ Voight components of 3.5 and 2.7 eV FWHM, respectively, at −46.3 and −43.4 eV (0.8 eV Gaussian, and 3.3 and 2.5 eV Lorentzian, respectively) with an area ratio Ru $4p_{1/2}$:Ru $4p_{3/2}$ of 0.4, the Ru layer appears oxide free when deposited at room temperature on HfO_2.[17] Finally, Fig. 5(d) shows SXPS spectra of the Si 2p core levels. This signal is attributed to a silicon suboxide at the Si interface with HfO_2 (Ref. 14) and is observable because the HfO_2 layer is so thin. Interestingly, this peak is also affected by the Ru deposition and exhibits a positive-energy shift of 0.5 eV.

In summary, upon deposition of metallic Ru on HfO_2, all the electronic density of states related to HfO_2 as well as the suboxide interface core level exhibit a rigid positive shift of 0.5 eV.

C. Ru/15 Å $Hf_{0.7}Si_{0.3}O_2$/Si

Similar to the HfO_2 film described above, the $Hf_{0.7}Si_{0.3}O_2$ sample studied here was 15 Å in thickness and was grown at

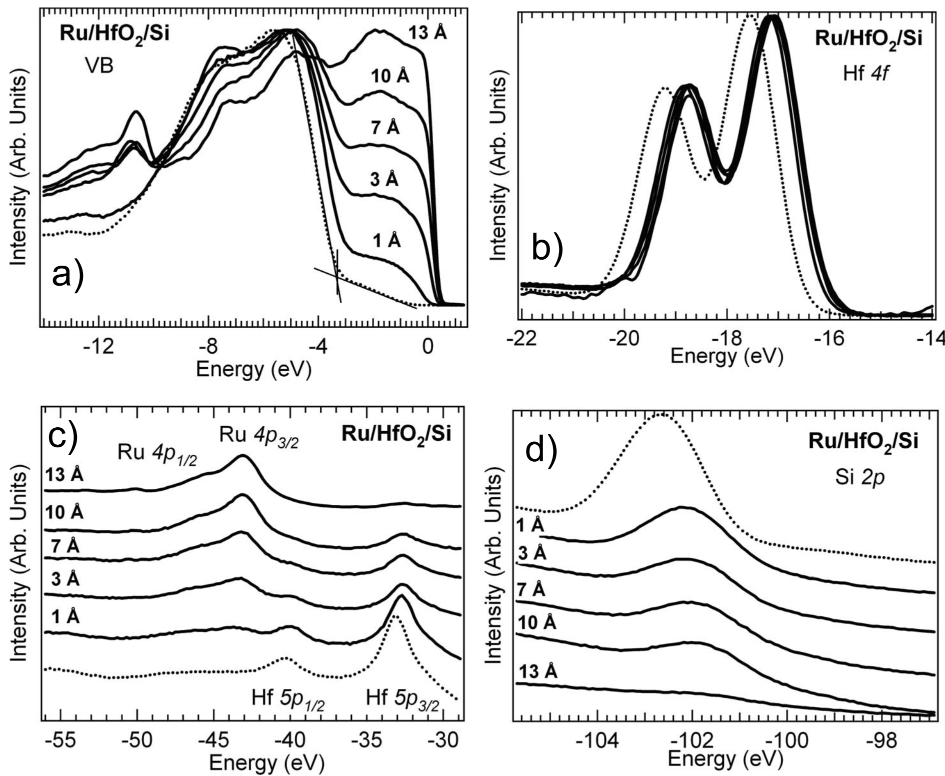

FIG. 5. (a) Valence-band, and (b) Hf 4f, (c) Ru 4p, and (d) Si 2p core levels measured at a photon energy of $h\nu$=150 eV of a 15 Å HfO_2/Si sample before and during sequential metallization with Ru. The spectra are referenced with respect to the silicon midgap position of the pristine sample.

SEMATECH by ALD on a p-doped Si with a resistivity of 1–2 Ω cm^{-1}.

The evolution of the VB and CB during Ru sequential depositions is shown in Figs. 6(a) and 6(b), respectively. The $Hf_{0.7}Si_{0.3}O_2$ electronic structure is intermediate between the ones of SiO_2 and HfO_2, with a valence band of O 2p character and a strong Hf 5d contribution for the conduction band. Before metallization, the positions of the VB and CB edges are −3.4 and −2.6 eV, respectively, giving a 6.0 eV gap.[14] As previously observed for the HfO_2 sample, the deposition of a 2 Å layer of Ru induces a rigid shift of the VB and CB edges estimated to be +0.4 eV.

For this sample, XPS was performed on the clean oxide[14] but not during sequential metallization. However, the absence of surface contamination was confirmed using AES. The similarity between the UPS and IPS spectra from HfO_2 and $Hf_{0.7}Si_{0.3}O_2$, particularly in terms of the line shape changes in the VB and CB shifts upon metallization, suggest that +0.4 eV is a good estimate of the band-edge shift induced when Ru is deposited onto $Hf_{0.7}Si_{0.3}O_2$.

D. Ru/25 Å Al_2O_3/Si

As a final comparison to an alternative high-κ dielectric, we performed direct and inverse photoemission measurements of a 25-Å-thick Al_2O_3 sample grown by ALD on a p-doped Si with a resistivity of 0.006 Ω cm^{-1}.

Valence-band photoemission spectra, obtained at the photon energy $h\nu$=40.8 eV, and IPS spectra of the conduction band, measured at an electron energy E_p=23.3 eV, are shown in Figs. 7(a) and 7(b), respectively, of a 25 Å Al_2O_3/Si upon sequential Ru metallization. The dotted curves are spectra from the clean oxide film while the solid curves are data from the metallized surfaces. The energy scales of the spectra are referenced to the silicon midgap of the pristine sample. The Ru thickness is also indicated for each metallization cycle. In a previous publication,[14] we have reported the position of the valence-band (mostly of O 2p character) and conduction-band (a mixture of Al 3s and Al 3p characters) edges for the clean oxide surface to be −3.8 and +3.2 eV with respect to the silicon midgap position. This gives a band gap of 7.0 eV for this Al_2O_3 film. After the first 3 Å of Ru were deposited on the oxide, a shift of the valence-band edge, estimated to be +0.3 eV, is observed. In addition, significant spectral intensity, and a well-defined Fermi edge, develops above the valence-band edge. As shown in Fig. 7(b), strong emission from unoccupied Ru 4d states develops near the Fermi level. As the cross section of the Al 3s and 3p states in the oxide CB is very low in comparison to the Ru states, it is not possible to evaluate a CB shift, even for the thinnest Ru overlayer.

SXPS spectra of the valence band, and the Al 2p and Ru 4p core levels from the Ru-metallized Al_2O_3 film are reported in Figs. 8(a)–8(c), respectively. As the smallest coverage studied here was 4 Å of Ru, the presence of strong Ru states prevents evaluation of shifts in the valence-band spectra. However, this shift can be determined precisely from the Al 2p core levels shown in Fig. 8(b). The Al 2p peak of the clean oxide is comprised of two components, the Al 2$p_{3/2}$ and Al 2$p_{1/2}$ lines, found at binding energies of 74.4 and 74.8 eV, respectively, with 1.3 eV Gaussian and 0.2 eV Lorentzian contributions for the width in good agreement with previous work. Similar to what was observed for the other oxides of this study, after the first Ru deposition the Al 2p core level exhibits a positive-energy shift of +0.3 eV. An examination of the Ru 4p core levels of Fig. 8(c) during sequential depo-

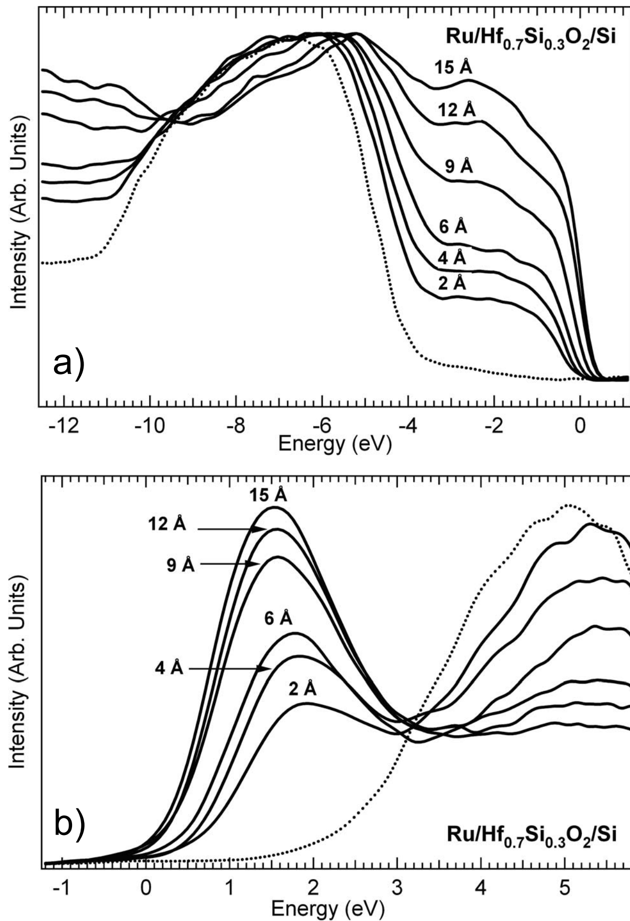

FIG. 6. (a) UPS ($h\nu$=40.8 eV) and (b) IPS (E_p=20.3 eV) spectra of the VB and CB band edges, respectively, during sequential metallization of a 15 Å $Hf_{0.7}Si_{0.3}O_2/Si$ with Ru. The spectra are referenced with respect to the silicon midgap position of the pristine sample.

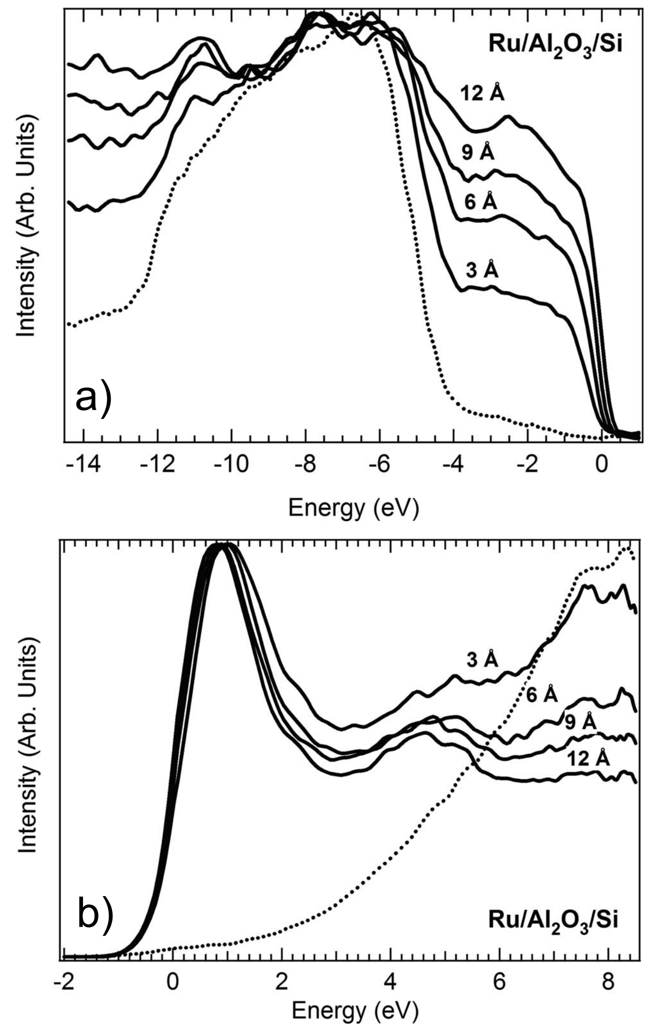

FIG. 7. (a) UPS ($h\nu$=40.8 eV) and (b) IPS (E_p=23.3 eV) spectra of the VB and CB band edges, respectively, during sequential metallization of a 20 Å Al_2O_3/Si with Ru. The spectra are referenced with respect to the silicon midgap position of the pristine sample.

sition of Ru confirms that Ru is not oxidized upon deposition at room temperature on Al_2O_3. Once again, the Ru $4p$ core levels have all of the features of the metallic state, and thus oxidation of Ru upon deposition does not occur at room temperature.[17]

IV. DISCUSSION

A. Experimental results

From the results reported in Sec. III, a systematic trend can be observed. Ru deposition at room temperature on any of the oxides studied here (SiO_2, HfO_2, $Hf_{0.7}Si_{0.3}O_2$, and Al_2O_3) occurs without strong chemical interaction with the substrate: there is no observable oxidation of the Ru gate or reduction in the ultrathin oxides. However, upon Ru deposition all the oxide-related peaks exhibit a positive-energy shift of a few tenths of an eV. If most of the core-level shift occurs even for low Ru coverage, the nominal value of the core-level shift is reached only after the first two or three Ru deposition cycles, where the metallic character of the Ru film is indicated by the presence of density of states at the Fermi level. (Note that the Fermi level of the system was measured independently on a gold or silver sample in contact with the sample.) At that point, the vacuum work function measured for Ru on all the samples was found to be 5.2 eV.

The measured band offsets (VBO_{meas} and CBO_{meas}) between the oxide and the Ru Fermi level is directly obtained by adding the oxide core-level shift (ΔE) observed upon Ru deposition to the position of the CBM or VBM of the clean oxide with respect to the measured Fermi level (VBM_{FL} and CBM_{FL}, respectively). These values are reported in Table I. Note that, for $Hf_{0.7}Si_{0.3}O_2$, the shift indicated was measured using the VB and CB data.

It has to be noted that in the case of $Ru/HfO_2/Si$, a significant core-level shift is also observed for the interfacial SiO_2 oxide with respect to their position for the pristine HfO_2/Si sample. This interfacial oxide core-level shift could be observed only through this thin 15 Å HfO_2 sample and generalization of this observation to the other samples studied here should be treated cautiously. This suggests that, however, dipole creation at the metal or oxide interface will

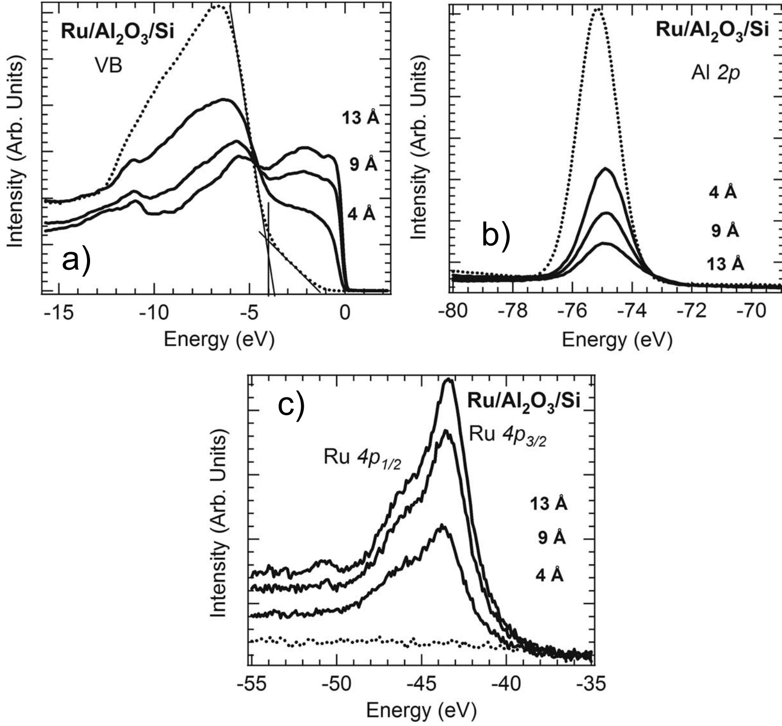

FIG. 8. (a) Valence-band, and (b) Al $2p$ and (c) Ru $4p$ core levels measured at a photon energy of $h\nu = 150$ eV of a 20 Å Al_2O_3/Si sample before and during sequential metallization with Ru. The spectra are referenced with respect to the silicon midgap position of the pristine sample.

induce some amount of electric field in both HfO_2 and SiO_2, the extent of which cannot be easily characterized.

Few systematic experimental results exist in the literature for the determination of the band alignment of Ru on oxides. High effective work functions have been determined for Ru on high-κ/Si stacks by electrical characterization [capacitance-voltage (CV) and current-voltage (IV)].[19–22] A commonly used method in determining band alignment of a metal gate with respect to an oxide substrate is to perform CV measurements on MOS stacks for varying oxide thicknesses. The determination of the flatband voltage V_{FB} as a function of the oxide thickness, th_{ox}, leads, by extrapolation to $th_{ox}=0$, to the metal gate effective work function $\phi_{M,\mathrm{eff}}$:

$$\phi_{M,\mathrm{eff}} = \phi_{\mathrm{Si}} + qV_{\mathrm{FB}} - \frac{Q_{\mathrm{ox}} \mathrm{th}_{\mathrm{ox}}}{\varepsilon_{\mathrm{ox}}}, \tag{6}$$

where q is the electronic charge, Q_{ox} represents the fixed charges in the oxide, ε_{ox} is the oxide permittivity, and ϕ_{Si} is a silicon work function defined as the difference between the vacuum and bulk Fermi levels of the silicon substrate.

Because it includes the interface dipole effects, $\phi_{M,\mathrm{eff}}$ is not directly comparable to the work function measured using UPS, ϕ_M. However, within the MIGS model, the CBO can be obtained as

$$\mathrm{CBO} = \phi_{M,\mathrm{eff}} - \chi_{\mathrm{O}}. \tag{7}$$

We can now compare the CV and IV results to this work. Ťapajna *et al.*[19] report the effective work function of metal-organic chemical-vapor deposition (MOCVD)-grown Ru at 300 °C on SiO_2, Al_2O_3, and HfO_2 to be 5.1, 5.0, and 5.3 eV, respectively. Using our experimentally measured oxide electron affinities, χ_O,[14] (see Table II) of 1.3, 2.5, and 2.5 eV, respectively, the CBOs are determined to be 3.8 eV for SiO_2, 2.5 eV for Al_2O_3, and 2.8 eV for HfO_2, from these electrical measurements. While for SiO_2 there appears to be perfect agreement between the value determined in this work and that found by the electrical measurements, this is not the case for the two others oxides, Al_2O_3 and HfO_2. As better agreement is found for the well characterized and virtually defect free SiO_2/Si system, the differences between these CBO measurements and those of the other oxides could be the

TABLE I. Measured band shift (Sh) upon Ru deposition, valence-band maximum (VBM_{FL}) and conduction-band maximum (CBM_{FL}) of the clean oxides with respect to the Fermi level, and VBO (VBO_{meas}) and CBO (CBO_{meas}) of the oxides with respect to Ru. All the reported values are given in eV.

	ΔE	VBM_{FL}	VBO_{meas}	CBM_{FL}	CBO_{meas}
SiO_2	0.2	−5.3	5.1	3.6	3.8
HfO_2	0.5	−3.8	2.4	1.9	2.4
$Hf_{0.7}Si_{0.3}O_2$	0.4[a]	−4.0	3.6	2.0	2.4
Al_2O_3	0.3	−4.3	4.0	2.7	3.0

[a]Shift obtained from the VB and CB spectra.

TABLE II. Comparison between the experimental and MIGS calculated CBOs using a CNL position rescaled to our experimental gap.

	S	$Egap_{meas}$ [a]	ϕ_O	χ_O [a]	CBO_{th}	CBO_{meas}
SiO_2	0.86[b]	8.9	5.1	1.3	3.9	3.8
HfO_2	0.53[c]	5.7	4.7	2.5	2.5	2.4
$Hf_{0.7}Si_{0.3}O_2$	0.56[c]	6.0	4.7	2.8	2.4	2.4
Al_2O_3	0.63[c]	7.0	5.1	2.5	2.7	3.0

[a]Reference 14.
[b]Reference 6.
[c]Reference 3.

result of either slight differences in the film quality, or, perhaps more importantly, the inability to properly model the contribution of the interfacial SiO_2 in the electrical measurements from Al_2O_3 and HfO_2. Also, in a subsequent work using a combination of electrical measurements and XPS, Ťapajna *et al.*[20] report the possibility of oxidation of their MOCVD-grown Ru films upon deposition at 300 °C. A better agreement for the CBO of HfO_2 with Ru is found in Suh *et al.*,[21] where a 5.02 eV effective work function for Ru leads to a 2.5 eV CBO (using our experimental value of the electron affinity for HfO_2).

A common difficulty in using electrical methods to determine band alignment is that a number of assumptions have to be made, from modeling the electrical response to the use of experimental values (energy gaps or electron affinities) obtained with different experimental techniques on slightly different samples. Following that idea, the set of data presented here is more comprehensive and direct for CBO determination. However, there is still a need for determining the driving forces that establish the band alignment. In Sec. IV B, we will compare these experimental results to the MIGS model.

B. Comparison with the MIGS model

In order to compare our experimental values to the MIGS model's predicted values, it is important to understand the nature of the parameters involved in this model, and in particular the pinning parameter S and the charge neutrality level (CNL).

The S parameter is correlated with the electronic part of the dielectric constant of the oxide (ε_∞) and has been found empirically to be well described by the relation:[7,8,13]

$$S = \frac{1}{1 + 0.1(\varepsilon_\infty - 1)^2}. \tag{8}$$

The S parameter is thus a bulk parameter obtained from an experimental value of ε_∞.[13] The CNL is defined as the position in the gap where evanescent states have an equivalent weight of CB and VB characters. The CNL is obtained from an *ab initio* calculated density of states for a given material.[3,6] The calculated CNL strongly depends on the nature of the model (crystalline oxide vs amorphous) and on the size of the energy gap. In the following work, we have chosen the values of S and CNL calculated by Robertson[3] (and Demkov *et al.*[6] for SiO_2) as a basis. However, because in this work the authors are using theoretical band-gap values ($Egap_{th}$) that are somewhat different than the ones we report from these ultrathin films ($Egap_{meas}$), and because the position of the CNL is directly affected by the relative position in energy of the occupied and unoccupied states, we rescale the theoretical position of the CNL (CNL_{th}) with respect to our measured gap values to find a CNL more suitable to our measured samples (CNL_{meas}):

$$CNL_{meas} = CNL_{th}\frac{Egap_{meas}}{Egap_{th}}. \tag{9}$$

The effective work function of the oxide is then given by

$$\phi_O = Egap_{meas} + \chi_O - CNL_{meas}. \tag{10}$$

According to Eqs. (3) and (10), using the experimentally measured oxide gap $Egap_{meas}$,[14] electron affinity χ_O,[14] and metal work function ϕ_M, in conjunction with theoretically determined S parameter and CNL position,[3,6] it is possible to calculate the conduction-band offset between an oxide and a metal. Using our measured work function of 5.2 eV for Ru, we are reporting values for the calculated CBOs (CBO_{th}) that can be directly compared to the CBOs measured in this work (CBO_{meas}) in Table II.

From this table it is clear that the measured CBO is in general in excellent agreement with the one predicted by the MIGS model rescaled to the experimental gap we measured, with errors on the order of our experimental uncertainties. For Al_2O_3, a possible explanation for the slightly larger measured CBO compared to the MIGS model prediction could be coming from the evaluation of the S parameter, obtained from an α-alumina phase.[3]

The agreement between the experimental determination of the band alignment and the MIGS model brings other questions. Indeed, the MIGS model assumes a perfect interface between the two materials, and the calculated parameters are evaluated assuming defect free materials. The interface bonding and coordination between two solids could be expected to have a strong influence on the band alignment, as it has been calculated recently for a HfO_2/SiO_2 interface.[23] The presence of defects such as oxygen vacancies in oxide films has also been shown to modify the band alignment in oxide/SiO_2/Si stacks between the oxide and the substrate by values of up to 2 eV.[24] In this work, the morphology of the Ru layer, obtained by physical vapor deposition, has not been investigated, and no electrical characterization was per-

formed on these stacks. As we do not anticipate having defect free oxides, we can conclude that in our case the band alignment between the Ru gate and the different oxides seems insensitive to these parameters. Possible explanations for the excellent agreement with the MIGS model are that the Ru growth is homogeneous enough, or that the possible defects in the ultrathin oxides films were passivated (maybe with hydrogen) upon exposure to air before introduction into the UHV experimental chambers.

V. CONCLUSION

In this work, we have determined the band alignment of a Ru gate with SiO_2, and with the more technologically relevant ultrathin high-κ oxides that are HfO_2, $Hf_{0.7}Si_{0.3}O_2$, and Al_2O_3. The CBO between Ru and the different dielectrics, obtained using UPS and IPS, are in reasonable agreement with the available numbers in the literature.[19–22] For the Ru/high-$\kappa/SiO_2/Si$ system, the MIGS model, where the CNL position is rescaled to an experimentally measured gap, gives a good description of the band alignment. These results are in contrast with what has been found for other metals such as Al, for which interfacial Al_2O_3 layer has been shown to develop upon metallization of other high-κ stacks, thus preventing a simple use of the MIGS model.[25] Due to its low oxygen affinity, Ru does not disrupt the high-$\kappa/SiO_2/Si$ stack upon deposition by creating an interfacial RuO_x layer, and appears as a good metal model for MIGS testing.

Ru growth at room temperature, using physical vapor deposition, is metallic on all the ultrathin oxides studied here. This is much different from other studies where Ru was grown at 300 °C by MOCVD, and where Ru oxide was formed.[20] For comparison with the behavior of Ru when integrated in devices, further experiments should include a characterization of the Ru gate stability while annealing in reducing or oxidizing atmosphere.

ACKNOWLEDGMENTS

The authors acknowledge the generous support of the Semiconductor Research Corporation and the National Science Foundation. We are grateful for the beam time allocation at the NSLS. The National Synchrotron Light Source, Brookhaven National Laboratory, is supported by the U.S. Department of Energy, Office of Science, Office of Basic Energy Sciences, under Contract No. DE-AC02-98CH10886.

[1] G. D. Wilk, R. M. Wallace, and J. M. Antony, J. Appl. Phys. **89**, 5243 (2001).
[2] E. P. Gusev, V. Narayanan, and M. M. Frank, IBM J. Res. Dev. **50**, 387 (2006).
[3] J. Robertson, J. Vac. Sci. Technol. B **18**, 1785 (2000).
[4] I. De, D. Johri, A. Srivastava, and C. Osburn, Solid-State Electron. **44**, 1077 (2000).
[5] K. Mistry *et al.*, Tech. Dig.-Int. Electron Devices Meet, 247 (2007).
[6] A. A. Demkov, L. R. C. Fonseca, E. Verret, J. Tomfohr, and O. F. Sankey, Phys. Rev. B **71**, 195306 (2005).
[7] J. Tersoff, Phys. Rev. Lett. **52**, 465 (1984a).
[8] J. Tersoff, Phys. Rev. B **30**, 4874 (1984b).
[9] W. Schottky, Phys. Z. **41**, 570 (1940).
[10] N. F. Mott, Proc. Cambridge Philos. Soc. **34**, 568 (1938).
[11] V. Heine, Phys. Rev. **138**, A1689 (1965).
[12] J. Bardeen, Phys. Rev. **71**, 717 (1947).
[13] W. Mönch, Phys. Rev. Lett. **58**, 1260 (1987).
[14] E. Bersch, S. Rangan, R. A. Bartynski, E. Garfunkel, and E. Vescovo, Phys. Rev. B **78**, 085114 (2008).
[15] D. Arena, F. Curti, and R. Bartynski, Surf. Sci. **369**, L117 (1996).
[16] E. Vescovo, H.-J. Kim, Q.-Y. Dong, G. Nintzel, D. Carlson, S. Hulbert, and N. V. Smith, Synchrotron Radiat. News **12**, 10 (1999).
[17] N. Mårtensson and R. Nyholm, Phys. Rev. B **24**, 7121 (1981).
[18] M. Ulrich, J. G. Hong, J. E. Rowe, G. Lucovsky, A.-Y. Chan, and T. E. Madey, J. Vac. Sci. Technol. B **21**, 1777 (2003).
[19] M. Ťapajna, P. Písečny, R. Lupták, K. Hušeková, K. Fröhlich, L. Harmatha, J. Hooker, F. Roozeboom, and J. Jergel, Mater. Sci. Semicond. Process. **7**, 271 (2004).
[20] M. Ťapajna, K. Hušeková, J. P. Espinos, L. Harmatha, and K. Fröhlich, Mater. Sci. Semicond. Process. **9**, 969 (2006).
[21] Y.-S. Suh, H. Lazar, B. Chen, J.-H. Lee, and V. Misra, J. Electrochem. Soc. **152**, F138 (2005).
[22] T. Nabatame, K. Segawa, M. Kadoshima, H. Takaba, K. Iwamoto, S. Kimura, Y. Nunoshige, H. Satake, T. Ohishi, and A. Toriumi, Mater. Sci. Semicond. Process. **9**, 975 (2006).
[23] O. Sharia, A. A. Demkov, G. Bersuker, and B. H. Lee, Phys. Rev. B **75**, 035306 (2007).
[24] C. Fulton, G. Lucovsky, and R. Nemanich, Appl. Phys. Lett. **84**, 580 (2004).
[25] S. Rangan, E. Bersch, R. A. Bartynski, E. Garfunkel, and E. Vescovo, Appl. Phys. Lett. **92**, 172906 (2008).